consequently we could make definite assignments with regard to the sodium (and the potassium) system from the results. First, lithium should bond even more strongly with acetone than would sodium. Therefore, failure to detect mass 65 ($Li^+ \cdot$acetone) in the lithium experiments enabled mass 81 in the sodium work to be attributed to $NaOH_2^+$(NaOH). Second, results with lithium revealed a peak at mass 31 and mass 49. Neither could arise from impurities in the apparatus and confirmed the formation of $Li^+ \cdot LiOH$ (31) and $LiOH_2^+ \cdot LiOH$ (49).

These results are especially exciting as they confirm the formation and, indeed, the stability of ions involving alkali metals co-clustered with both their corresponding hydroxides, and at the same time water. Another important finding is that the dimer ion of sodium clustered with one water molecule can form in the high pressure reaction source. As seen in Table 2, mass 64 could not be attributed to an impurity and is identified as $Na_2^+(H_2O)$. No higher-order clusters of water about Na_2^+ exist. A related interesting aspect of the results is that no mass 32 ($Li_2^+ \cdot H_2O$) is formed; the first cluster containing two lithium atoms has an attached OH group rather than an H_2O molecule. The reaction of the alkali metal dimer ion with one water molecule is apparently exothermic for the case of lithium to form $Li^+ \cdot LiOH$, but requires the addition of a second water molecule in the case of sodium and potassium. This interpretation implies that the bond energy between an alkali metal ion and its corresponding hydroxide is relatively large. Based on thermochemical considerations, the findings indicate that the values exceed ~2eV; this is in accord with expectations considering the large dipole moments of the alkali hydroxides. Clearly, these results experimentally confirm the suggested interpretation of the atmospheric measurements[1]. Note that solely on a mass basis an alternative interpretation of the NPH ions observed in the stratosphere would be sodium chloride cluster ions of the form $Na^+(NaCl)_x(H_2O)_y$. Values of x from 0 to 2, and y from 0 to 5 allow an assignment for all NPH ions reported. Experiments are in progress in our laboratory to investigate the possibility of the proposed switching reactions and the bond energies for the species identified in this study.

Support of NASA under grant NSG 2248, the Atmospheric Sciences Section of the NSF under grant ATM 79-13801, and the Österreichischer Fonds zur Förderung der Forschung under grant S-18/08 is acknowledged. The Cooperative Institute for Research in Environmental Sciences is jointly sponsored by the University of Colorado and the National Oceanic and Atmospheric Administration.

Table 2 Ion clusters observed in high pressure mass spectrometric studies* of sodium utilizing a thermionic source||

Mass	Proposed identification	Mass	Proposed identification
23	Na^+	113	Na^+(DME)
41	$Na^+(H_2O)$		$Na^+(H_2O)_5$
59	$Na^+(H_2O)_2$	117	$NaOH_2^+$(NaOH)·$(H_2O)_2$
64†	$Na_2^+(H_2O)$	121	$Na^+(H_2O)_3 \cdot (CO_2)$
67	$Na^+(CO_2)$	131	Na^+(DME)·(H_2O)
77	$Na^+(H_2O)_3$		$Na^+(H_2O)_6$
81‡	$NaOH_2^+$(NaOH)	135	$NaOH_2^+$(NaOH)·$(H_2O)_3$
85	$Na^+(H_2O)\cdot(CO_2)$	139	$Na^+(H_2O)_4(CO_2)$
95	$Na^+(H_2O)_4$		[$NaOH_2^+$(NaOH)$_2$·(H_2O)]§
99	$NaOH_2^+$(NaOH)·(H_2O)	143	$NaOH_2^+$(NaOH)·$(H_2O)\cdot(CO_2)$
103	$Na^+(H_2O)_2\cdot(CO_2)$	149	Na^+(DME)·$(H_2O)_2$
111	$Na^+(CO_2)_2$		$Na^+(H_2O)_7$

*Experiments were also made with argon and nitrogen as carrier gas, and with deuterated water, to confirm the mass identifications.

†It is unlikely that the observed mass 64 is due to Na^+ attached to an impurity of mass 41 as we would then also expect to see $Na^+(41)(H_2O)$ of mass 82.

‡Corresponds in mass to $Na^+ \cdot$acetone. This possibility was discounted on the basis of experiments with lithium where no mass 65 ($Li^+ \cdot$acetone) was detected.

§A possible contributor to the more predominant species involving water and carbon dioxide.

|| Present studies.

Received 4 February; accepted 15 April 1980.

1. Ferguson, E. E. *Geophys. Res. Lett.* **5**, 1035 (1978).
2. Arnold, R., Krankowsky, D. & Marien, K. H. *Nature* **267**, 30 (1977).
3. Fehsenfeld, F. C., Dotan, I., Albritton, D. L., Howard, C. J. & Ferguson, E. E. *J. geophys. Res.* **83**, 1333 (1978).
4. Arnold, R., Böhringer, H. & Henschen, G. *Geophys. Res. Lett.* **5**, 653 (1978).
5. Arijs, E., Ingels, J. & Nevejans, D. *Nature* **271**, 642 (1978).
6. Castleman, A. W. Jr, Holland, P. M., Lindsay, D. M. & Peterson, K. I. *J. Am. chem. Soc.* **100**, 6039 (1978).
7. Castleman, A. W. Jr *Kinetics of Ion Molecule Reactions* (ed. Ausloos, P.) (Plenum, New York, 1979).
8. Castleman, A. W. Jr *Advances in Colloid and Interface Science* Vol. 10 (ed. Zettlemoyer, A.) 73 (Elsevier, Oxford, 1979).

Heat flow in the Mesozoic and Cenozoic

Donald Sprague & Henry N. Pollack

Department of Geological Sciences, The University of Michigan, Ann Arbor, Michigan 48109

The present-day heat flow from the Earth has commonly been used to estimate the abundance of heat-producing isotopes within the Earth. However, if heat flow has a variability on a short time scale (compared with the isotopic decay times), then the present-day heat flow must be seen as a much coarser measure of the Earth's heat-producing isotopic content. We report here the results of an investigation into the likely variation in terrestrial heat flow over the past 180 Myr.

The empirical relationships between the terrestrial heat flux and the age of oceanic crust or the age of last tectonothermal mobilization of continental crust[1,2] (Fig. 1) can be used to estimate the global heat flux, provided the age distribution of the crust is known[3]. Various recent estimates[4–6] of the present-day mean terrestrial heat flow fall in the range $81 \pm 3\,mW\,m^{-2}$. We present here a probabilistic model of crustal age distributions and heat flow from the present to the early Mesozoic. The model is based on the present-day distribution of crustal ages (see Table 1) and an estimate of the probability that crust produced or tectonothermally mobilized at an earlier time will have survived to the present day.

To determine the age distribution of the oceanic crust at a past time t, oceanic lithosphere which accreted between time t and the present must be subtracted from the present-day distribution, and lithosphere which has been subducted in the same interval must be reinstated; the age of the resurrected lithosphere is, however, uncertain, and must be estimated.

We define an age distribution at time t according to $Q_s(t,\tau)d\tau = Q_0(\tau)d\tau \cdot P_s(t,\tau)$, where $Q_s(t,\tau)d\tau$ is the area of crust of age τ surviving at time t. $Q_0(\tau)d\tau$ is the original area of crust accreted along oceanic ridges at time τ in the time interval $d\tau$, and P_s is a survival probability function giving the probability that crust accreted at time τ survives (has not been subducted) at the later time t. If the total area of oceanic crust is at all times constrained to be equal to the present-day area A_0, then production and survival can be related by

$$P_s(t,\tau) = 1 - \left[\frac{\int_t^\tau Q_0(\tau)d\tau}{\alpha A_0}\right]^{1/(\alpha-1)}$$

in which α is the number of present-day oceanic areas produced by ocean ridge accretion during the past 180 Myr. The mean accretion rate over this period is therefore $\alpha A_0/180$. As the area of ocean accreted between times τ and t increases, the survival probability decreases, finally becoming zero. The original area accreted at time τ is estimated from the

0028-0836/80/230393-03$01.00

Table 1 Percentage of global area represented by crust of indicated age

Ocean		Continent	
Age (Myr)	%	Age (Myr)	%
0–5	3.5	0–65	4.6
5–23	10.9	65–225	5.8
23–38	6.9	225–400	9.2
38–65	10.2	400–600	9.1
65–100	21.2	600–2,500	7.7
100–135	5.4	2,500–3,500	2.0
135–180	3.5		
Total	61.6		38.4

Continental shelves are included as continents of early and late Palaeozoic age.

present-day crustal distribution $Q_s(0,\tau)d\tau$ by $Q_0(\tau)d\tau = Q_s(0,\tau)d\tau/P_s(0,\tau)$. As crust older than any now present (>180 Myr) is needed to complete the ocean floor, the mean of $Q_0(\tau)$ from 180 Myr to the present is used.

The form of $P_s(t,\tau)$ is an arbitrary choice. We have tried other smooth, monotonically decreasing functions which satisfy the constraint that the accretion–subduction process yields the present-day area A_0. We find that the heat flow history is much more strongly dependent on the mean accretion rate, that is the choice of α, than on the particular functional form of P_s.

Tectonic processes affecting continents are significantly different from oceanic processes. While there is an increasing probability that old ocean crust will not survive, the same cannot be said for old continental crust. In fact, the survival of extensive areas of continental crust for more than 3,000 Myr testifies to the contrary. Old continental lithosphere is cool, thick, strong and refractory, and moreover tends to be centrally located in continental masses and is thus less frequently affected by plate margin interactions. Accordingly, we have assigned to continental areas a probability of tectonothermal remobilization that decreases exponentially with time since the previous mobilization. In contrast to old crust, recently mobilized continental crust has a high probability of being remobilized, for example in terrains above long-lived subduction zones. Another consideration is that continental mobilizations are not independent of oceanic accretion rates. Intervals of fast accretion must be accompanied by increased subduction with concomitant effects on continental margins. Formally, the calculation of area of continental crust of age τ at time t takes the form $Q_c(t,\tau)d\tau = \beta Q_0(\tau)\exp[-(\tau-t)/t_c]d\tau$, where the constants β and t_c are evaluated by the requirement that Q_c yield the present-day areas of Cenozoic and Mesozoic terrains. The values of β and t_c so determined are 0.15 and 100 Myr, respectively. The constant t_c is the time constant for the decay of probability of continental remobilizations.

The heat flow in both oceanic and continental regions can thus be calculated from the age distributions $Q_s(t,\tau)$ and $Q_c(t,\tau)$, and the empirical heat flow–age relationships of Fig. 1. An infinite set of possible models obtains in principle from the inherent variability allowed by the relationship between the production rate of oceanic crust and its subsequent probability of survival. All such models yield the present-day distribution of ages (Table 1) and hence the present-day distribution of oceanic heat flow. In application, however, practical constraints such as past spreading rates as deduced from marine magnetic anomalies limit the allowable models to the range $1.5<\alpha<3.5$. Our preferred model, shown in Fig. 2 and for which $\alpha=2.4$, in addition correctly predicts the present-day mean age of subducting crust, 77 Myr. For the range of α cited above, the mean age of subduction ranges from 111 to 60 Myr, thus providing a moderately sensitive guide to the choice of a proper α and a preferred model.

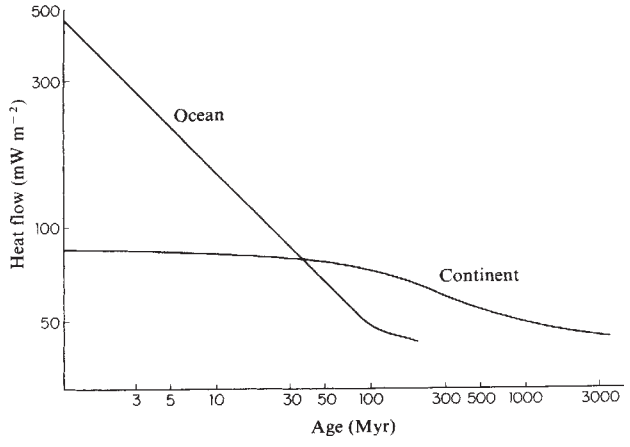

Fig. 1 Heat flow versus age relationships for oceans[1] and continents[2].

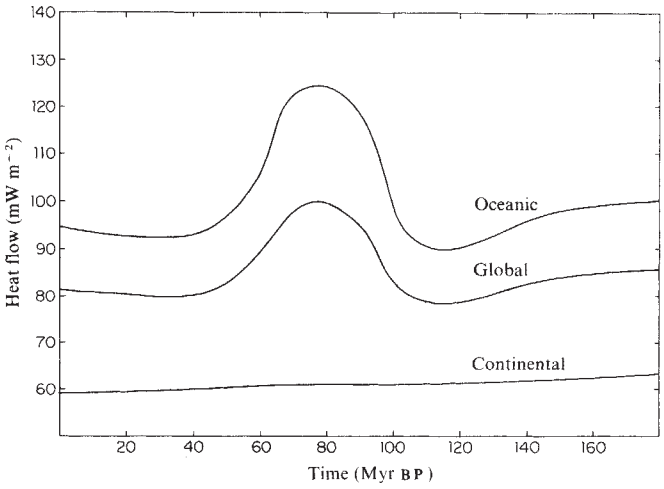

Fig. 2 Variability of mean oceanic, continental and global heat flow over the past 180 Myr.

The mean accretion rate over the past 180 Myr for this model is such that in that interval 2.4 times the present oceanic area has been produced, of which 1.4 has been subducted. Numerically this mean accretion rate is $1.33\%\ A_0$ Myr^{-1}, slightly above but comparable with estimates of the present-day accretion rate of 0.91–$1.14\%\,A_0\,Myr^{-1}$. (The lower value is derived from 'present-day' relative rotation vectors for the world plate system[7]; the upper value is derived from the amount of ocean floor produced in the past 5 Myr.) As shown in Fig. 2, the global heat flux varies between 78 and 101 $mW\,m^{-2}$, although for all but 40 Myr the heat flow is within $\pm 5\,mW\,m^{-2}$ of the 81 $mW\,m^{-2}$ present-day flux. The mean of the global heat flow over the 180 Myr interval is 85 $mW\,m^{-2}$, slightly above the present-day value. The principal feature of the heat flow history is the peak occurring in the late Cretaceous fast spreading episode; the minimum heat flow occurred in the early Cretaceous just before the opening of the South Atlantic Ocean. Clearly, nearly all of the variation in the global heat flux is due to the oceanic component. This results because of the greater area of ocean, the more extreme variation of heat flow with age in the oceans, and the greater impact of variations in oceanic accretion rate on oceanic heat flow than on continental heat flow.

We conclude that heat flow over the past 180 Myr has been in the range 78–101 mW m^{-2}. Throughout most of this period the heat flow was close to the present-day value of 81 mW m^{-2}; the only significant departure was the increase to the peak value of 101 mW m^{-2} during the rapid seafloor spreading of the late Cretaceous. The mean heat flow over the 180 Myr interval is 85 mW m^{-2}, somewhat in excess of the present-day vaue.

This research was supported in part by the Division of Earth Sciences, NSF, under grant EAR 78-09131.

Received 28 December 1979; accepted 14 March 1980.

1. Parsons, B. & Sclater, J. G. *J. geophys. Res.* **82**, 803–827 (1977).
2. Chapman, D. S. & Furlong, K. *EOS Trans. Am. geophys. Un.* **58**, 1240 (1977).
3. Chapman, D. S. & Pollack, H. N. *Earth planet. Sci. Lett.* **28**, 23–32 (1975).
4. Williams, D. L. & Von Herzen, R. P. *Geology* **2**, 327–328 (1974).
5. Sclater, J. G., Jaupart, C. & Galson, D. *Rev. geophys. Space Phys.* **18**, 269–311 (1980).
6. Davies, G. *Rev. geophys. Space Phys.* (in the press).
7. Minister, J. B. & Jordan, T. H. *J. geophys. Res.* **83**, 5331–5354 (1978).

Cambrian stromatolitic phosphorites from the Georgina Basin, Australia

P. N. Southgate

Research School of Earth Sciences, Australian National University, PO Box 4, Canberra, ACT 2600, Australia

The first details of Phanerozoic stromatolitic phosphorites are reported here. The stromatolites, from the Thorntonia Limestone in the Georgina Basin, northern Australia are of middle Cambrian age. The carbonates interfinger with and underlie the Beetle Creek Formation which contains Australia's largest known phosphate deposits. Phosphatic stromatolites had previously only been found in Proterozoic rocks, from the middle to upper Riphean Aravalli Group of Rajasthan, India and in the USSR and China[1]. It was generally considered that phosphatic stromatolites were unique to the Precambrian[2,3]. Indeed this unique association had led to hypotheses that during the Precambrian a different set of phosphogenic processes must have existed[4].

The Georgina Basin is a large epicontinental basin dominated by platform carbonates ranging in age from the early middle Cambrian to the middle Ordovician. On a regional scale the middle Cambrian sequence represents a complex facies mozaic consisting of carbonates, evaporites, phosphorites and terrigenous clastics (Fig. 1). The early middle Cambrian transgression is represented by a basal clastic interval which overlies the Precambrian basement. This interval is overlain by the Thorntonia Limestone and its lateral facies equivalents. The stromatolites occur in the Thorntonia Limestone; a carbonate unit consisting of stylolitic vuggy recrystallized dolomite and dolomitic limestone of Ordian to Templetonian age[5]. Minor diastems are common throughout the unit occurring as scalloped surfaces[6] and as phosphatized hardgrounds which were emergent for brief periods. The phosphatized stromatolites overlie minor dissolution surfaces and hardgrounds.

Although stromatolites occur at various localities within the Georgina Basin[7], phosphatic stromatolites are only known within 1–4 m thick discontinuous stromatolitic beds, ~10 km south of Riversleigh Station (Fig. 1). Preservation of algal laminae and internal fabric is variable and depends on the type of replacement. Silicification and particularly dolomitization obscure the primary algal structure but where stromatolites are phosphatic both columnar and laminar form are preserved.

Phosphatic stromatolitic columns up to 4 cm high or phosphatic cryptalgalaminite up to 5 cm thick are found overlying minor dissolution surfaces within the Thorntonia Limestone. Phosphatic laminae up to 2 mm thick occur discontinuously near the basal parts of the stromatolites and immediately overlying minor erosional surfaces within the stromatolitic bioherms. Chert-replaced laminae are not related

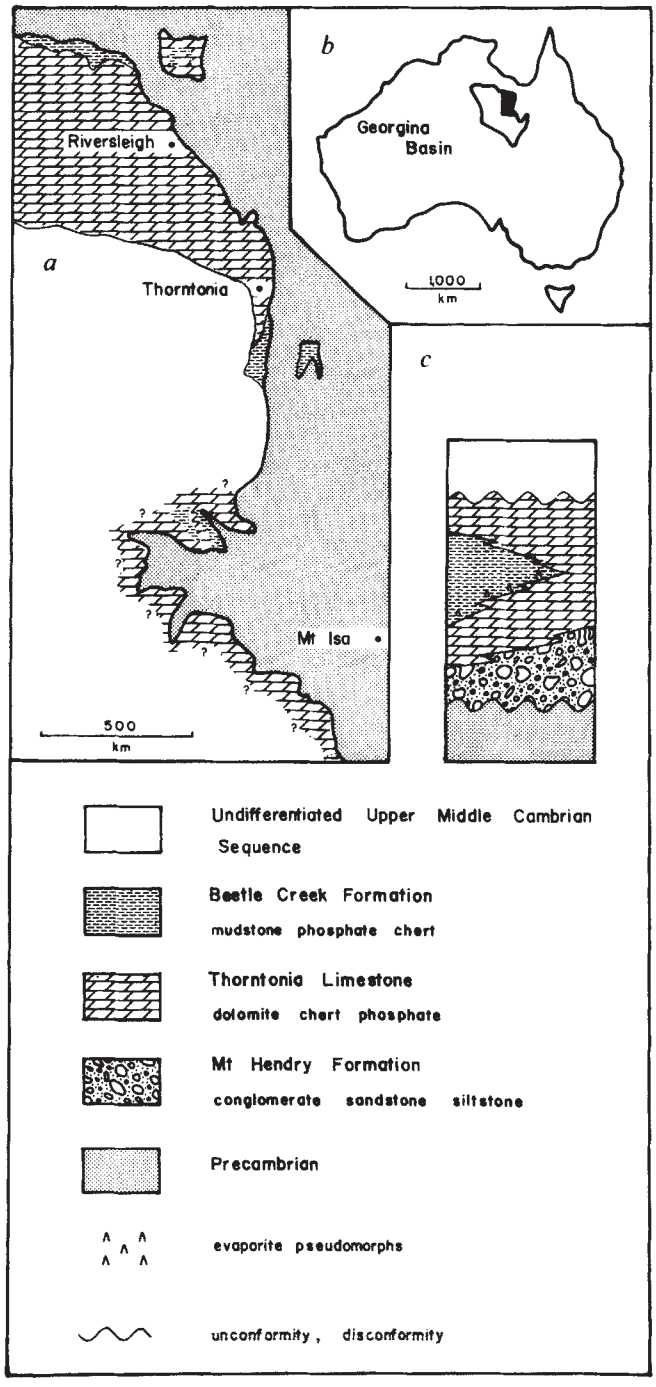

Fig. 1 *a*, map showing the northeastern margin of the Georgina Basin and the close lateral relationship between outcrop of Thorntonia Limestone and Beetle Creek Formation. *b*, Location map for the Georgina Basin, the north-east portion shown in *a*. is shaded. *c*, Generalized stratigraphic column for the lower middle Cambrian sequence of the northeastern Georgina Basin.

0028–0836/80/230395–03$01.00